Available online at www.sciencedirect.com

SciVerse ScienceDirect

Ceramics International 38 (2012) 2647–2652

CERAMICS INTERNATIONAL

www.elsevier.com/locate/ceramint

# Synthesis and electrochemical properties of $LiV_3O_8$ via an improved sol–gel process

Dunqiang Wang, Liyun Cao, Jianfeng Huang *, Jianpeng Wu

*Key Laboratory of Auxiliary Chemistry and Technology for Light Chemical Industry, Ministry of Education, Shaanxi University of Science and Technology, Xi'an 710021, PR China*

Received 27 October 2011; received in revised form 11 November 2011; accepted 11 November 2011
Available online 22 November 2011

**Abstract**

$LiV_3O_8$ cathode material was synthesized via a hydrothermal improved sol–gel process using LiOH, $NH_4VO_3$ and oxalic acid as raw materials. The thermal decomposition process of the as-prepared $LiV_3O_8$ precursor was investigated by thermogravimetric (TG) and differential scanning calorimetry (DSC). The structure, morphology and electrochemical performance of the as-synthesized $LiV_3O_8$ samples were characterized by X-ray diffraction (XRD), Fourier transform infrared (FT-IR), scanning electron microscopy (SEM) and the galvanostatic charge–discharge test. The effects of synthesis conditions on phases, structure and electrochemical performance of the $LiV_3O_8$ samples were particularly discussed. Result shows that pure $LiV_3O_8$ sample can be obtained at 300 °C, which is much lower than that of normal citric assisted sol–gel method. The sample synthesized at 350 °C exhibits the best electrochemical performance, which can present an initial discharge capacity of 301.1 mAh/g at a current density of 50 mA/g and maintain 271.6 mA/g (about 90.2% of its initial value) after 10 cycles.


*Keywords:* Sol–gel processes; Batteries; $LiV_3O_8$; Electrochemical properties

## 1. Introduction

Lithium vanadium oxide ($LiV_3O_8$) is a promising cathode material for rechargeable lithium batteries, which has been extensively studied over the past two decades for its attractive electrochemical properties such as high specific energy, good rate capacity, long cycle life, facile preparation and low cost [1,2].

$LiV_3O_8$ has a layered structure composed of two basic structural units, $VO_6$ octahedra and $VO_5$ distorted trigonal bipyramids [3]. There are two different sites for lithium ions, octahedron and tetrahedron. Lithium ions generally occupy the octahedral sites. As more lithium ions intercalate into the host compound, extra lithium ions may enter the tetrahedral sites. More than 3 $Li^+$ ions per formula can be inserted into this compound [4]. The lithium ions that occupy the octahedral sites linked to the $V_3O_8$ layer by strong ionic bonds, this makes the crystal structure of $LiV_3O_8$ stable during the charge–discharge process. Despite its structural advantages, it was found that the electrical properties of $LiV_3O_8$ strongly depend on the synthesis method and synthesis conditions under which the cathode material is prepared. Up to date, a large number of efforts have been done to prepare $LiV_3O_8$ crystallites with the aim to improve its discharge capacity and cycle stability, such as solid-state reaction [5], low temperature method [6], hydrothermal reaction [7,8], microwave assisted solid-state synthesis [9], sol–gel process [10–14], microwave assisted sol–gel method [15,16], combustion method [17], ultrasonic treatment [18], spray drying synthesis [19], freeze drying technique [20], spray pyrolysis process [21].

As a promising way, sol–gel method has been extensively used to synthesize cathode material due to their unique advantages such as low synthesis temperature, high purity and high homogeneous structure and good electrochemical property of the synthesized product. Many works have been done to fabricate $LiV_3O_8$ crystallites by using sol–gel methods in which citric acid was mostly used as chelating agent. In sol–gel process, it will take several hours to finish the reaction of sol formation. In recent decades, microwave hydrothermal have been developed to synthesize inorganic materials due to its

* Corresponding author. Tel.: +86 029 86168803; fax: +86 029 86168803.
*E-mail addresses:* wongdq1986@163.com (D. Wang), hjfnpu01@163.com (J. Huang).

0272-8842/$36.00 
doi:10.1016/j.ceramint.2011.11.030

advantages such as facilely reaction control, high energy utilization, effective reaction and time saving. It is well known that oxalate compounds often have low decomposition temperature, thus it is easy to synthesize $LiV_3O_8$ by simply sintering the precursor at low temperature. In the present work, we synthesized the $LiV_3O_8$ crystallites via a microwave hydrothermal improved sol–gel process with oxalic acid as chelating agent. The influence of synthesis conditions on the phase composition, structure and electrochemical performance of the as-synthesized samples were discussed in detail.

## 2. Experimental

### 2.1. Sample preparation

All the chemical reagents used in the experiment were of analytical grade and used without any purification. Stoichiometric amounts of $LiOH{\cdot}H_2O$ and $NH_4VO_3$ (Li:V = 1:3, molar ratio) were mixed in deionized water and the solution of oxalic acid was added to the mixture under constant magnetic stirring. The molar ratio of oxalic acid to total amount of metal ions was 2:1. The resultant solution was then transferred to a 100 mL Teflon-lined autoclave. The autoclave was heated at 140 °C and maintained for 30 min under the microwave hydrothermal system (MDS-8, Shanghai Sineo Microwave Chemistry Technology Co. Ltd., China). After the microwave hydrothermal treatment, the autoclave was cooled to room temperature naturally and a blue solution was obtained. Next, the solution was placed at 80 °C for 12 h to form a gel. The gel was washed with absolute ethyl alcohol twice to remove the remaining water with a later drying in a vacuum oven at 120 °C for 5 h to obtain the precursor. Finally the precursor was ground and then calcined at 300, 350, 400 and 500 °C for 4 h to produce the powders, respectively. After cooling to room temperature naturally in the furnace, the powders were reground to obtain the $LiV_3O_8$ products.

### 2.2. Characterization

The thermal decomposition process of the precursor was analyzed by thermogravimetric and differential scanning calorimeters (TG-DSC, NETZSCH STA 409PC) thermal analyzer at the heating rate of 15 °C/min in air from room temperature to 700 °C. The crystal structures of the as-prepared powders were investigated by X-ray diffractometry (XRD, Rigaku D/max-2000) with a graphite monochromatic Cu Kα radiation ($\lambda = 0.15418$ nm) in the $2\theta$ range of 5–70°. The morphology and particle size of the samples were observed by scanning electron microscopy (SEM, JEOL JSM-6460). The bonding nature of the samples was obtained by Fourier transform infrared (FT-IR, Bruker VERTEX 70) absorption spectra.

### 2.3. Electrochemical measurements

In order to prepare the working electrode for the electrochemical measurements, the $LiV_3O_8$ powders (85 wt%), polyvinylidene difluoride (10 wt%) and acetylene black (5 wt%) were ground and dispersed in N-methyl pyrrolidone (NMP). The mixture was stirred for 12 h to form slurry and then pressed onto a pure Al foil, dried at in vacuum at 120 °C for 24 h. The cells were assembled in an argon-filled glove box with the concentrations of moisture and oxygen below 1 ppm, lithium foil as anode and Celgard 2320 film as separator. The electrolyte was 1 M $LiPF_6$ in ethylene carbonate (EC) and dimethyl carbonate (DMC) in volume ratio of 1:1. The capacity and cycling performance of the electrode were performed on a galvanostatic charge–discharge cycle test using Land battery measurement system (CT2001A, Wuhan, PR China) at a current density of 50 mA/g in the potential range of 2.0–4.0 V (vs. $Li^+/Li$). All the tests were performed at room temperature.

## 3. Results and discussion

### 3.1. Thermal analysis

Fig. 1 shows the TG-DSC curves of the as-prepared $LiV_3O_8$ precursor. It is found that the thermal decomposition of the precursor can be divided into three steps. The first one is from room temperature to about 260 °C with weight loss of ~15 wt% and no obvious peak is observed on the DSC curve except the evaporation of residual water and chemical bound water in the precursor. The mass loss increases as the process of heating is continued. A rapid weight loss (~55 wt%) in the second step from 260 to 360 °C indicates the combustion and decomposition of the precursor have been strongly happened. The strong and sharp exothermic peak at 320 °C on the DSC curve may be attributed to decomposition of the remnants precursor and crystallization of $LiV_3O_8$. The last step is from 360 to 700 °C with a weight loss of ~3 wt%. A big and wide exothermic peak is observed in the range of 480–550 °C on the DSC curve, which may result from the further crystallization of $LiV_3O_8$. The weight loss may be attributed to the lag decomposition of the residual precursor. There is no obvious weight loss after 600 °C. At about 610 °C, an obvious endothermic peak is observed on the TG-DSC curve but the weight of the sample

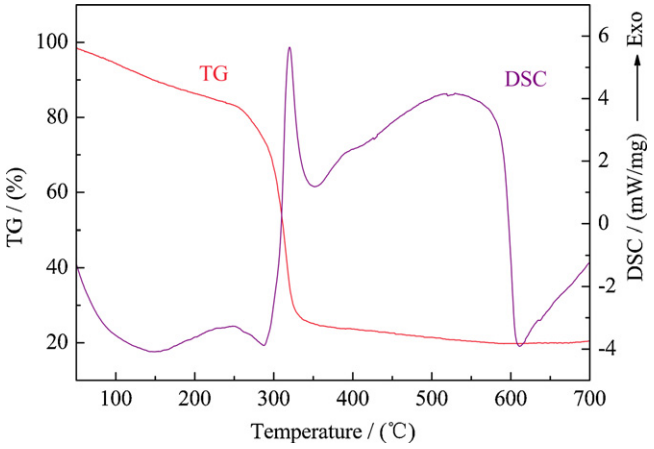


Fig. 1. TG-DSC curves of the as-prepared $LiV_3O_8$ precursor.

keeps constant, this should be ascribed to the melting of $LiV_3O_8$. The different crystallinity and structure of the $LiV_3O_8$ would be obtained at different calcination temperatures. Therefore, the range of temperature is selected in 300–500 °C for our experiments.

### 3.2. XRD analysis

XRD patterns of the $LiV_3O_8$ samples prepared at different temperatures are shown in Fig. 2. It can be seen that the diffraction peaks of all the samples are well identified as the typical layered structure corresponding to the $LiV_3O_8$ (JCPDS No. 72-1193) without out any impurities, which means that the as-synthesized $LiV_3O_8$ crystallites have a single monoclinic crystalline structure and belong to the P21/m space group. This shows that pure $LiV_3O_8$ sample can be obtained at 300 °C, which is much lower than that of normal citric assisted sol–gel method [11,14]. According to XRD data, the calculated lattice parameters of all samples are listed in Table 1, which are close to the reported values [5,16]. The lager $d_{100}$ means the wider interlayer space, which could facilitate the mobility and distribution of lithium ions between layers, and follows the improvement of the electrochemical performance such as specific capacity and cycle stability. The main difference of the four patterns is the relative intensity of the (1 0 0) and (1 0 3) peaks. And it is found that there are only weak XRD peaks observed at 300 °C, the intensity of (1 0 3) peak is nearly the same as that of (1 0 0) peak. The broader and lower diffraction peaks of the sample may be attributed to its small crystallites and low crystallinity, which will be shown later by SEM results. The (1 0 0) peak becomes higher and sharper over other peaks with the increase of temperature, which indicates higher crystallinity and more preferred orientation growth along (1 0 0) plane of $LiV_3O_8$. To $LiV_3O_8$ with layer structure, the higher intensity of (1 0 0) peak will cause stronger (1 0 0) plane preferred orientation and relatively long diffusion paths for lithium ions, which is disadvantageous to reversible insertion/extraction of $Li^+$ ions between the $(V_3O_8)^-$ layers.

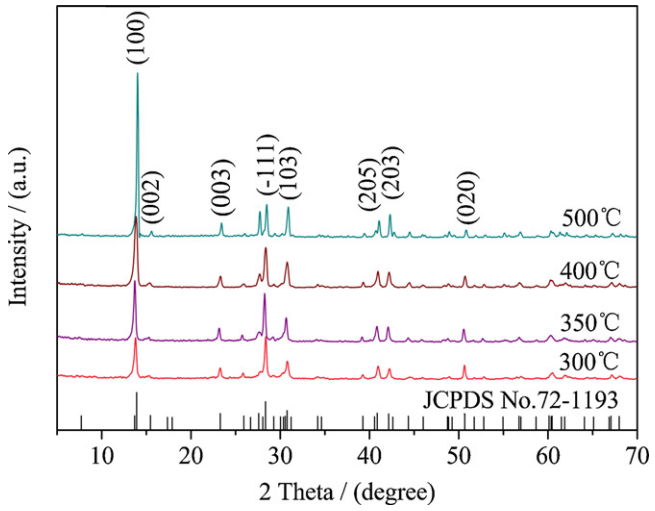


Fig. 2. XRD patterns of the $LiV_3O_8$ samples prepared at different temperatures.

Table 1
Lattice parameters of the $LiV_3O_8$ synthesized at different temperatures.

| Samples (Å) | 300 °C | 350 °C | 400 °C | 500 °C |
|---|---|---|---|---|
| $a_0$ | 6.6499 | 6.6702 | 6.6613 | 6.6714 |
| $b_0$ | 3.6024 | 3.6085 | 3.5949 | 3.5925 |
| $c_0$ | 11.9946 | 12.0268 | 12.0133 | 12.0423 |
| $d_{100}$ | 6.3354 | 6.3519 | 6.3438 | 6.3406 |

The effect of Li/V molar ratio on the phase composition of $LiV_3O_8$ was also studied. Fig. 3 illustrates the XRD patterns of the $LiV_3O_8$ samples synthesized at 350 °C with different Li/V molar ratios ($R$). It is clear that the patterns of the samples synthesized at $R = 0.75{:}3$ and $R = 1.00{:}3$ are similar, both of which show pure $LiV_3O_8$. With the increase of $R$, impurity phase presents. The sample shows $LiVO_3$ impurity phase when $R$ is 1.25:3, while that prepared at $R = 1.50{:}3$ shows both $LiVO_3$ and $LiV_{15}O_{35.5}$ impurity phase. This may be because that pure $LiV_3O_8$ can be obtained at a proper Li/V molar ratio, excessive lithium ions lead to the formation of impurities during the calcination process.

### 3.3. FTIR analysis.

The bonding nature of the $LiV_3O_8$ samples prepared at different calcination temperatures for 4 h was studied by FTIR. The FT-IR spectra of the $LiV_3O_8$ samples are shown in Fig. 4. The FT-IR absorption in the wavelength of 400–1200 $cm^{-1}$ has five main peaks around 999, 974, 956, 750 and 551 $cm^{-1}$, respectively. The former three peaks are corresponded to the stretching vibration of V=O bonds and the fourth peak is assigned to the stretching vibration of V–O–V in the crystal cell [22,23]. The last peak is attributed to the bending vibration of V=O and V–O–V symmetric stretching [9]. The intensity and position of some peaks show a little difference due to the dissimilar crystal growth behavior. It can be seen that the sample obtained at 500 °C shows no peak at 750 $cm^{-1}$, however, it shows a clear peak at 599 $cm^{-1}$, which may be

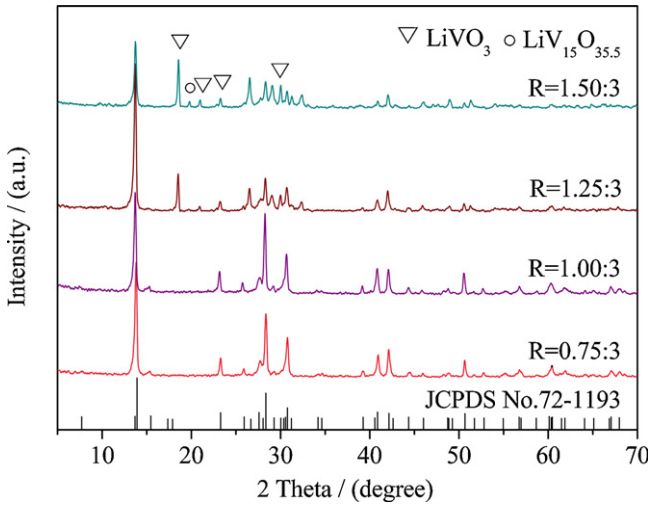


Fig. 3. XRD patterns of the $LiV_3O_8$ synthesized at 350 °C with different Li/V molar ratios (R).

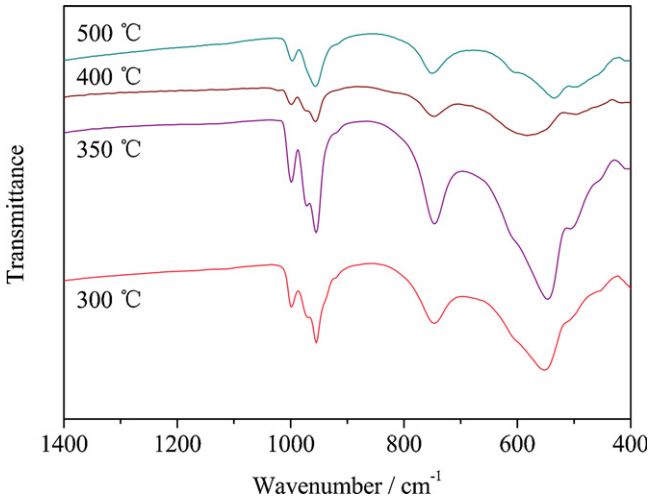


Fig. 4. FT-IR spectra of the $LiV_3O_8$ samples prepared at different calcination temperatures.

attributed to its crystal growth orientation along (1 0 0) plane. This is in agreement of the XRD results.

### 3.4. SEM analysis

Fig. 5 shows the SEM images of the $LiV_3O_8$ samples synthesized at different temperatures. It reveals that the calcination temperature has a significant effect on the morphology and particle size of the as-synthesized $LiV_3O_8$ crystallites. The sample prepared at 300 °C shows irregular morphology and small particle with low crystallinity, the average diameter of the particles is ~400 nm. The morphology of the sample obtained at 350 °C exhibits thin sheet-like structure with thickness of 50–200 nm, 100–500 nm in width and 0.5–3 μm in length. With the increase of calcination temperature, the morphology of the sample changes to rod-like structure, the particle size gradually increases and the edges of the particles become much sharper. This may be attributed to the preferred orientation along (1 0 0) plane and the secondary particles growth with increasing temperature. This is in good agreement with the above analysis. It has been shown by several researchers that the morphology can have a significant effect on electrochemical performance of the $LiV_3O_8$ samples. And it is well known that the intercalation process of lithium ions between the layers of the cathode is a diffusion process. Therefore the smaller particles and lower crystallinity of the $LiV_3O_8$ sample have relatively short diffusion paths for the intercalation of lithium ions between $(V_3O_8)^-$ layers, which may lead to higher specific capacity and better cycle stability. Therefore the $LiV_3O_8$ prepared at 300 and 350 °C should have better electrochemical performance.

### 3.5. Electrochemical properties

The initial charge–discharge curves of the $LiV_3O_8$ samples prepared at different temperatures at the current density of 50 mA/g are illustrated in Fig. 6. It can be seen that there are three main discharge plateaus at 2.78, 2.64 and 2.48 V, which corresponds to the Li ions insertion into the cathode. This is the characteristic of the electrochemical process of $LiV_3O_8$. It shows that with the increase of calcination temperature, the discharge capacity of the samples decreases differently. The sample obtained at 300 °C shows the highest initial discharge capacity of 311.3 mAh/g. According to the formula of specific capacity ($C = nF/3.6$ M), for the samples prepared at 300, 350, 400 and 500 °C, there are about 3.34, 3.23, 3.06 and 2.86 mol $Li^+$ ions inserted into the material at the end of the discharge

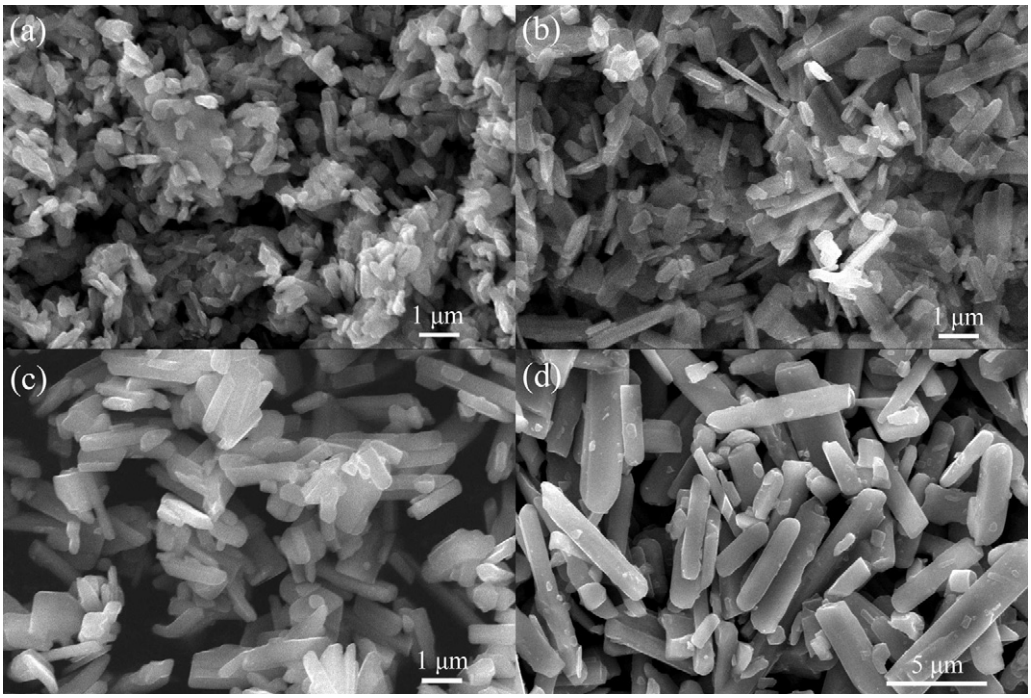


Fig. 5. SEM images of the $LiV_3O_8$ samples synthesized at different temperatures: (a) 300 °C; (b) 350 °C; (c) 400 °C; (d) 500 °C.

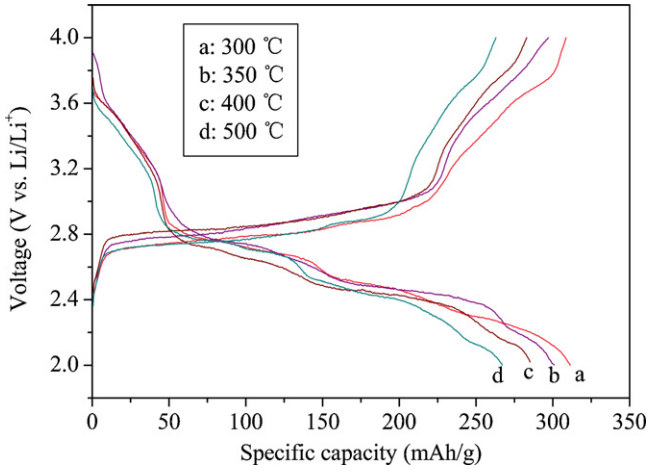


Fig. 6. The initial charge–discharge curves of the $LiV_3O_8$ samples prepared at different temperatures (a) 300 °C; (b) 350 °C; (c) 400 °C; (d) 500 °C.

process, respectively. The high discharge capacity of sample obtained at 300 °C may be attributed to its irregular morphology with smaller particle size and low crystallinity, which can make the efficient contact of the material with the electrolyte and provide more active sites for $Li^+$ ions diffusion. In contrast, the above results also suggest that the well-crystallized sample with preferred orientation and larger particle size does have poor specific capacity, which is in agreement with the previous studies [7,11].

Fig. 7 shows the cycling performance of the $LiV_3O_8$ samples synthesized at different temperatures in the potential range of 2.0–4.0 V (vs. $Li/Li^+$) at the current density of 50 mAh/g. Different capacity decay of these samples can be observed during the cycle process. The sample obtained at 300 °C presents an initial discharge capacity of 311.3 mAh/g and it drops to 262.4 mAh/g (about 84.3% of its initial value) after 10 cycles. The sample obtained at 350 °C exhibits a relatively lower capacity of 301.1 mAh/g compared with the former one, but it can maintain a capacity of 271.6 mAh/g (about 90.2% of its initial value), which shows a good cycling performance. And

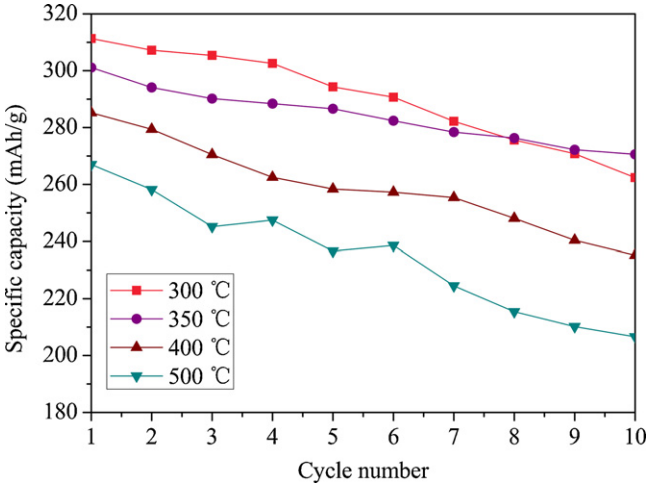


Fig. 7. The cycling performance of the $LiV_3O_8$ samples prepared at different temperatures.

the electrochemical performance of this sample is better than that prepared at the same temperature in the literature [24]. With increase of calcinations temperature, the cycle stability of the sample decreases. The capacities of sample prepared at 400 and 500 °C remain 235.2 and 206.6 mAh/g after 10 cycles corresponding to 82.4% and 77.3% of their initial values, respectively. The relatively worse electrochemical performance of the samples obtained at 400 and 500 °C may be attributed to their rod-like morphologies with preferred orientation and larger particle size, which is disadvantage for the electrolyte penetration and reversible $Li^+$ ions diffusion. Capacity decay probably results from the incomplete reversibility of phase transformation between the $LiV_3O_8$ and $Li_4V_3O_8$ [15,25], which indicates that the insertion/extraction of $Li^+$ ions during the cycle process of $LiV_3O_8$ is not completely reversible.

## 4. Conclusions

In summary, we have synthesized the $LiV_3O_8$ cathode material via a microwave hydrothermal improved sol–gel process with oxalic acid as chelating agent. Result shows that pure $LiV_3O_8$ sample can be obtained at 300 °C, which is much lower than that of normal citric assisted sol–gel method. The charge–discharge tests show that the sample synthesized at 350 °C exhibits a relatively high initial discharge capacity and good cycling stability. At a current density of 50 mA/g in the potential range of 2.0–4.0 V, the initial discharge capacity is 301.1 mAh/g and it maintains 271.6 mA/g (about 90.2% of its initial value) after 10 cycles. All this reveals that this synthesis routine is a promising method for preparing the $LiV_3O_8$ cathode material.

## Acknowledgments

This work was supported by the National Natural Science Foundation of China (50942047), Natural Science Foundation of Shaanxi Province of China (2010JM6001), International Science and Technology Cooperation Project of Shaanxi Province (2011kw-11), and the graduate Innovation Foundation of Shaanxi University of Science and Technology.

## References

[1] V. Manev, A. Momchilov, A. Nassalevska, G. Pistoia, M. Pasquali, A new approach to the improvement of $Li_{1+x}V_3O_8$ performance in rechargeable lithium batteries, J. Power Sources 54 (1995) 501–507.
[2] C. Cheng, Z.H. Li, X.Y. Zhan, Q.Z. Xiao, G.T. Lei, X.D. Zhou, A macaroni-like $Li_{1.2}V_3O_8$ nanomaterial with high capacity for aqueous rechargeable lithium batteries, Electrochim. Acta 55 (2010) 4627–4631.
[3] L.A. de Picciotto, K.T. Adendorff, D.C. Liles, M.M. Thackeray, Structural characterization of $Li_{1+x}V_3O_8$ insertion electrodes by single-crystal X-ray diffraction, Solid State Ionics 62 (1993) 297–307.
[4] J. Gao, C.Y. Jiang, C.R. Wan, Preparation and characterization of spherical $Li_{1+x}V_3O_8$ cathode material for lithium secondary batteries, J. Power Sources 125 (2004) 90–94.
[5] Y.M. Liu, X.C. Zhou, Y.L. Guo, Structure and electrochemical performance of $LiV_3O_8$ synthesized by solid-state routine with quenching in freezing atmosphere, Mater. Chem. Phys. 114 (2009) 915–919.

[6] A.M. Kannan, A. Manthiram, Low temperature synthesis and electrochemical behavior of $LiV_3O_8$ cathode, J. Power Sources 159 (2006) 1405–1408.
[7] H.Y. Xu, H. Wang, Z.Q. Song, Y.W. Wang, H. Yan, M. Yoshimura, Novel chemical method for synthesis of $LiV_3O_8$ nanorods as cathode materials for lithium ion batteries, Electrochim. Acta 49 (2004) 349–353.
[8] J.Q. Xu, H.L. Zhang, T. Zhang, Q.Y. Pan, Y.H. Gui, Influence of heat-treatment temperature on crystal structure, morphology and electrochemical properties of $LiV_3O_8$ prepared by hydrothermal reaction, J. Alloys Compd. 467 (2009) 327–331.
[9] G. Yang, G. Wang, W.H. Hou, Microwave solid-state synthesis of $LiV_3O_8$ as cathode material for lithium batteries, J. Phys. Chem. B 109 (2005) 11186–11196.
[10] Z.J. Wu, X.B. Zhao, J. Tu, G.S. Cao, J.P. Tu, T.J. Zhu, Synthesis of $Li_{1+x}V_3O_8$ by citrate sol–gel route at low temperature, J. Alloys Compd. 403 (2005) 345–348.
[11] L. Liu, L.F. Jiao, Y.H. Zhang, J.L. Sun, L. Yang, Y.L. Miao, H.T. Yuan, Y.M. Wang, Synthesis of $LiV_3O_8$ by an improved citric acid assisted sol–gel method at low temperature, Mater. Chem. Phys. 111 (2008) 565–569.
[12] H. Heli, H. Yadegaric, A. Jabbari, Low-temperature synthesis of $LiV_3O_8$ nanosheets as an anode material with high power density for aqueous lithium-ion batteries, Mater. Chem. Phys. 126 (2011) 476–479.
[13] H. Ma, Z.Q. Yuan, F.Y. Cheng, J. Liang, Z.L. Tao, J. Chen, Synthesis and electrochemical properties of porous $LiV_3O_8$ as cathode materials for lithium-ion batteries, J. Alloys Compd. 509 (2011) 6030–6035.
[14] H.L. Zhang, J.R. Neilson, D.E. Morse, Vapor-diffusion-controlled sol–gel synthesis of flaky lithium vanadium oxide and its electrochemical behavior, J. Phys. Chem. C 144 (2010) 19550–19555.
[15] F. Wu, L. Wang, C. Wu, Y. Bai, Structural characterization and electrochemical performance of lithium trivanadate synthesized by microwave sol–gel method, Electrochim. Acta 54 (2009) 4613–4619.
[16] F. Wu, L. Wang, C. Wu, Y. Bai, F. Wang, Study on $Li_{1+x}V_3O_8$ synthesized by microwave sol–gel route, Mater. Chem. Phys. 115 (2009) 707–711.
[17] Y.C. Si, L.F. Jiao, H.T. Yuan, et al., Structural and electrochemical properties of $LiV_3O_8$ prepared by combustion synthesis, J. Alloys Compd. 486 (2009) 400–405.
[18] Y.M. Liu, X.C. Zhou, Y.L. Guo, Effects of reactant dispersion on the structure and electrochemical performance of $Li_{1.2}V_3O_8$, J. Power Sources 184 (2008) 303–307.
[19] N. Tran, K.G. Bramnik, H. Hibst, J. Prölß, N. Mronga, M. Holzapfel, W. Scheifele, P. Novák, Spray-drying synthesis and electrochemical performance of lithium vanadates as positive electrode materials for lithium batteries, J. Electrochem. Soc. 155 (2008) A384–A389.
[20] O.A. Brylev, O.A. Shlyakhtin, A.V. Egorov, Y.D. Tretyakov, Phase formation and electrochemical properties of cryochemically processed $Li_{1+x}V_3O_8$ materials, J. Power Sources 164 (2007) 868–873.
[21] S.H. Ju, Y.C. Kang, Morphological and electrochemical properties of $LiV_3O_8$ cathode powders prepared by spray pyrolysis, Electrochim. Acta 55 (2010) 6088–6092.
[22] G. Yang, W.H. Hou, Z.Z. Sun, Q.J. Yan, A novel inorganic–organic polymer electrolyte with a high conductivity: insertion of poly(ethylene) oxide into $LiV_3O_8$ in one step, J. Mater. Chem. 15 (2005) 1369–1374.
[23] H.M. Liu, Y.G. Wang, W.S. Yang, H.S. Zhou, A large capacity of $LiV_3O_8$ cathode material for rechargeable lithium-based batteries, Electrochim. Acta 56 (2011) 1392–1398.
[24] L. Liu, L.F. Jiao, J.L. Sun, Y.H. Zhang, M. Zhao, H.T. Yuan, Y.M. Wang, Electrochemical properties of submicron-sized $LiV_3O_8$ synthesized by a low-temperature reaction route, J. Alloys Compd. 471 (2009) 352–356.
[25] J. Kawakita, T. Miura, T. Kishi, Charging characteristics of $Li_{1+x}V_3O_8$, Solid State Ionics 118 (1999) 141–147.